

## RESEARCH ARTICLE

# Brazing ZrB<sub>2</sub> ultra-high-temperature ceramics to Zr metals for hypersonic thermal protection systems

Younes Belrhiti<sup>1</sup>  | M. Watson Grossman<sup>1</sup> | R. Hedgecock<sup>1</sup> | M. McGilvray<sup>2</sup> | L. Vandeperre<sup>1</sup>

<sup>1</sup>Department of Materials, Imperial College London, London, UK

<sup>2</sup>Oxford Thermofluids Institute, University of Oxford, Oxford, UK

## Correspondence

Younes Belrhiti, Department of Materials, Imperial College London, London, UK.  
Email: [younes.belrhiti@gmail.com](mailto:younes.belrhiti@gmail.com)

## Abstract

Porous and dense zirconium diboride (ZrB<sub>2</sub>) materials are promising ultra-high-temperature ceramics (UHTCs) for transpiration cooling in hypersonic applications, providing an effective means to reduce component temperatures and mitigate oxidation effects. While porous ZrB<sub>2</sub> enables coolant flow, dense ZrB<sub>2</sub> offers structural integrity. However, achieving a reliable ceramic-to-metal connection remains a significant challenge due to the inherent differences in their physical, chemical, and mechanical properties. This study investigates the brazing process of both porous and dense ZrB<sub>2</sub> UHTCs to zirconium metal (Zr). Zr was selected due to its thermal expansion properties closely matching those of ZrB<sub>2</sub>, reducing thermal stress at the interface and enabling coolant transfer into porous ZrB<sub>2</sub> from the supply reservoir. The brazing temperature of 1650°C was selected based on the Zr–ZrB<sub>2</sub> phase diagram to ensure eutectic melting without compromising the structural integrity of the base materials, and the filler composition was selected to enhance wetting and spreading. The results demonstrate that dense ZrB<sub>2</sub> forms robust and continuous interfaces with Zr metal, while porous ZrB<sub>2</sub> presents greater challenges due to thermal expansion mismatches and paste infiltration. These findings provide valuable insights into ceramic–metal joining for aerospace high-performance thermal protection systems under extreme conditions, which would reinforce the real-world impact.

## KEYWORDS

brazing, ceramic–metal joining, hypersonic applications, transpiration cooling, UHTCs

## 1 | INTRODUCTION

Porous and dense zirconium diboride (ZrB<sub>2</sub>) materials are among the most promising ultra-high-temperature ceramics (UHTCs)<sup>1–6</sup> for extreme environment applications requiring alternative engineering approaches, partic-

ularly transpiration cooling in hypersonic applications.<sup>7</sup> This cooling technology involves passing a coolant fluid through porous materials to reduce the overall temperature of the component. Additionally, it can mitigate oxidation effects, a major challenge for most UHTCs in air environments.<sup>8,9</sup> This technology is particularly suitable

This is an open access article under the terms of the [Creative Commons Attribution](https://creativecommons.org/licenses/by/4.0/) License, which permits use, distribution and reproduction in any medium, provided the original work is properly cited.

© 2025 The Author(s). International Journal of Applied Ceramic Technology published by Wiley Periodicals LLC on behalf of American Ceramics Society.

for high-heat flux regions, such as leading edges or shock impingement zones, which are exposed to extreme thermal loads ( $>1 \text{ MW/m}^2$ ) due to the high velocities of hypersonic vehicles traveling through planetary atmospheres. In such extreme conditions, materials must withstand not only thermal loads but also intense mechanical and oxidative stresses encountered during planetary atmospheric re-entry and sustained hypersonic flight.<sup>10,11</sup>

In the studied application, the coolant needed to be transferred into the porous  $\text{ZrB}_2$  through a metallic tube connected to the supply reservoir to achieve effective cooling. While porous  $\text{ZrB}_2$  is critical for enabling this cooling mechanism, dense  $\text{ZrB}_2$  plays a complementary role by providing mechanical strength and thermal compatibility at structural interfaces, such as the junctions with metallic coolant channels. Establishing a reliable bond between ceramics and metals is crucial to fully exploit their complementary properties. While ceramics<sup>12,13</sup> exhibit excellent high-temperature performance, metals<sup>14</sup> provide superior toughness and mechanical strength. Ceramics and metals have considerable differences in physical, chemical, and mechanical properties, and so these advanced materials put forward new requirements for material joining techniques. Indeed, conventional fusion welding methods, such as arc,<sup>15</sup> electron beam,<sup>16</sup> and laser welding,<sup>17</sup> cannot be used to connect ceramics and metals effectively. Various joining techniques have been explored, such as ultrasonic bonding,<sup>18</sup> self-propagating high-temperature synthesis (SHS),<sup>19</sup> and partial transient liquid phase welding,<sup>20</sup> have been developed in recent years. However, current literature and practical applications indicate that brazing and diffusion welding are still the primary methods of connecting ceramics and metals.<sup>21–23</sup>

This paper focuses on the brazing process to join both porous and dense  $\text{ZrB}_2$  UHTCs with metals, aiming to create structurally sound interfaces for future deployment in hypersonic thermal protection systems. Zirconium (Zr) was selected due to its thermal expansion coefficient being close to that of  $\text{ZrB}_2$ , minimizing thermal stress mismatches between Zr and  $\text{ZrB}_2$ , thereby limiting residual stresses at the interface. The brazing temperature was carefully chosen to ensure that the filler material melts while preventing the base materials from reaching their melting points, thereby preserving their structural integrity and performance. Furthermore, the composition of the metallic filler paste was selected to achieve wetting and spreading at brazing temperature. Given the fundamental differences between ceramics (covalent bonding) and metals (metallic bonding), achieving continuous adhesion requires precise control over wettability, which is influenced by factors such as atmosphere, temperature, thermodynamic stability, alloy composition, and surface conditions to achieve continuous interfaces between  $\text{ZrB}_2$

and Zr metal were obtained. The conditions for this brazing process are detailed in this paper.

## 2 | EXPERIMENTAL

### 2.1 | Materials

Porous  $\text{ZrB}_2$  (35% porosity) were produced using  $\text{ZrB}_2$  powder (ABCR, grade A, 3–5 mm). The powder was partially oxidized by heating  $540^\circ\text{C}$  for 30 min before sieving and hot-pressing in an argon (Ar) atmosphere at  $1700^\circ\text{C}$  under 24 MPa for 15 min to prevent the oxidation of the powder. Pre-oxidizing the powder surface promotes structural coarsening and enhances necking between particles while preventing excessive densification at high temperatures. This results in a more open porous structure, which is desirable for transpiration cooling. Porous discs and porous hollow cylinders were manufactured and presented in Figure 1A.

Dense  $\text{ZrB}_2$  was produced by hot-pressing  $\text{ZrB}_2$  powders (ABCR, grade B, 1–3 mm) at  $2000^\circ\text{C}$  under 24 MPa, achieving a density of 95%. Dense  $\text{ZrB}_2$  hollow cylinders were manufactured (Figure 1A). The dense  $\text{ZrB}_2$  samples in this work were obtained by joining a dense  $\text{ZrB}_2$  cylinder to a porous  $\text{ZrB}_2$  disc using compression at high temperature ( $2100^\circ\text{C}$ ) using a small amount of a  $\text{ZrB}_2$  paste to facilitate bonding.

The  $\text{ZrB}_2$  cylinder was wire-cut using electrical discharge machining (EDM) around the partial thickness drill holes, and the rear collar was rough-cut away using wire EDM. The outer cylindrical surface was finished using a die-sink electrode. Pilot holes are wet-drilled with SiC bits (4 mm, then 6 mm) from RS components (UK supplier), and final finishing was achieved using 6.5 mm thin-wall diamond core drills.

Commercial Zr tubes (ZR00-TB-000200 with a purity of 99.2%) with an outside diameter of 6.35 mm, a wall thickness of 0.9 mm, and an inside diameter of 4.55 mm were used. The final sample geometry is detailed in Figures 1B,C.

### 2.2 | Paste preparation

Bonding between Zr tubes and  $\text{ZrB}_2$  was achieved using a glycerol-based paste containing submicron Zr(m) and  $\text{ZrB}_2$  powders in eutectic proportions of 86.3% Zr and 13.7% B which produces a liquid phase when fired at  $1650^\circ\text{C}$ , as indicated by the phase diagram represented in Figure 2. Any intermediate paste composition would also form a eutectic melt, but controlling the reaction kinetics is crucial to limiting erosion of both the metal and ceramic. The

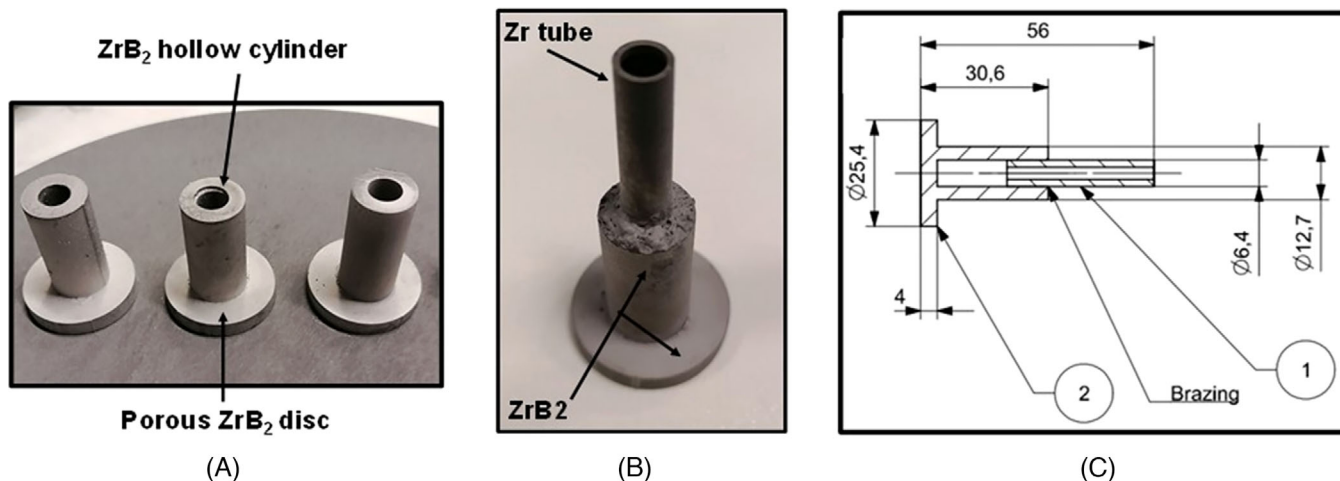


FIGURE 1 Brazed Zr tube with  $ZrB_2$  sample.

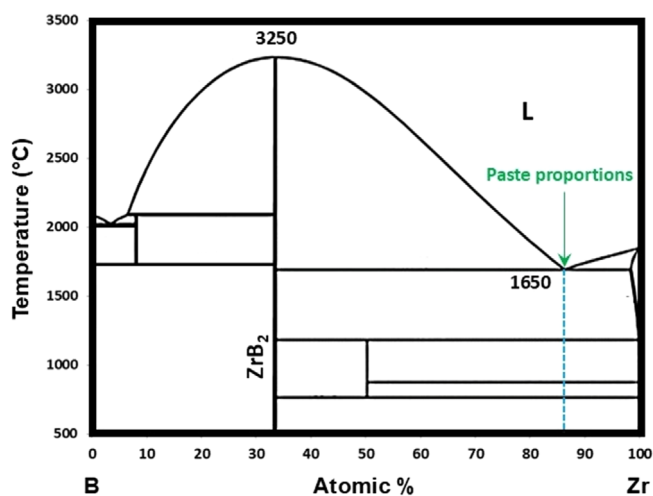


FIGURE 2 Zr-B phase diagram.

empirically optimized paste composition and sintering conditions provided a balance between bonding strength and reaction control at the interface.

Zr powder was mixed with  $ZrB_2$  powder as received (ABCR, grade B, 1–3  $\mu\text{m}$ ) using a mortar and pestle. A minimal amount of glycerol was then added to create a thick and sticky paste.

### 2.3 | Brazing process

A 10 mm section of the Zr tube was coated with the paste and introduced in the rear tube of the dense  $ZrB_2$  sample. Excess paste was scraped off the external surface while introducing the Zr tube inside the  $ZrB_2$  sample (Figure 2B). The sample was sintered at 1650°C (eutectic melt temperature of Zr and  $ZrB_2$ ) under vacuum ( $\sim 10^{-5}$  mbar),

using a heating ramp of 20°C/min and a dwell time of 20 min. During cooling to room temperature under vacuum (10°C/min), the molten filler solidified, forming a continuous bond without significant interfacial voids between the ceramic and metal<sup>24</sup> (Figure 1B).

### 2.4 | Leakage and pressure resistance testing

To validate the effectiveness of the brazed joint, compressed air was injected through the Zr tube into the sample at an applied pressure of 6.5 bar for 10 min, corresponding to the expected operational conditions of the final application. The Zr tube was tightly sealed at the compressed air inlet on one side, while the other end was joined to a dense or porous hollow cylindrical  $ZrB_2$  element, which was itself sealed to a porous  $ZrB_2$  disc as shown in Figure 1. A pressure gauge was connected to monitor the internal pressure buildup. The entire system was maintained in a closed configuration to simulate actual in-service conditions where pressurization would occur. Additionally, a soapy water solution was applied around the external interface during pressurization to detect any leakage through the bonding region.

### 2.5 | Microstructure characterization: scanning electron microscopy analysis

The sample was fully embedded in an epoxy resin (Buehler, EpoThin 2, 20-3440-032) with a resin-to-hardener ratio of 100:45. Sectional cuts were prepared for scanning electron microscopy (SEM) analysis including grinding, polishing, and the gold coating application on the analyzed surface.

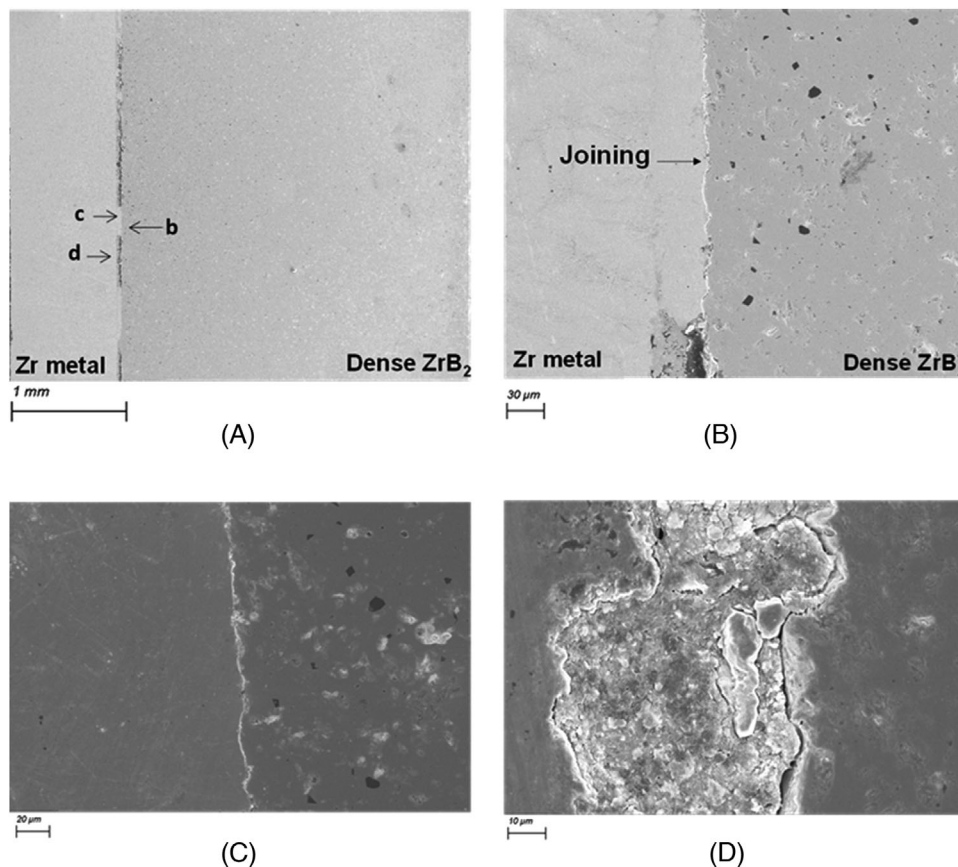


FIGURE 3 SEM analysis of dense  $ZrB_2$  brazed to Zr metal. SEM, scanning electron microscopy.

### 3 | RESULTS AND DISCUSSION

Figure 3 presents two SEM images of a vertical cross-section of the brazed sample, showing the interface between the Zr tube and the dense  $ZrB_2$ .

Figure 3A provides an overview of the central region of the sample with low-magnification SEM images showing the macrostructure of the joint between Zr metal (left) and dense  $ZrB_2$  (right), distinguishable. At a macroscopic scale, the bonding interface appears continuous; however, dark lines are locally observed along the interface, which are attributed to unreacted grains or potential microvoids, likely resulting from incomplete wetting or minor surface contamination. To avoid the presence of unreacted grains in the joint, it would be advantageous to sieve the Zr- $ZrB_2$  mixture before adding of glycol.

Figure 3B,C highlights higher-magnification SEM images which provide a detailed view of the interface region between the Zr metal and dense  $ZrB_2$  presented in Figure 3A. The continuous brazing line is visible without delamination. Figure 3D represents a close-up of a localized defect observed in Figure 3B. This feature does not correspond to a gap, but rather to unreacted grains

that remained during the brazing process likely resulting from a local wetting failure, surface contamination. The presence of such a defect indicates that, despite the overall integrity of the joint, localized bonding imperfections may occur due to the paste mixing homogeneity and so interfacial reactions.

The presence of submicron Zr(m) as an active element with a high melting point enhanced the wettability of the paste, promoting bonding between ceramic and metal, as evidenced by the absence of visible delamination. Additionally, the absence of significant gaps observed at the interface is attributed to the similar thermal behavior of both base materials at the brazing temperature ( $1650^\circ\text{C}$ ) and during the cooling phase.

The  $ZrB_2$ -Zr connection remained intact under 6.5 bar air pressure, with no observed leakage or delamination. Besides, no external bubbles from the soapy solution were detected in this region, confirming that the seal was effective and airtight to be used for the final application.

Two porous  $ZrB_2$  cylinders were brazed to the Zr tube to manufacture the porous brazed sample. A sectional cut of the first sample was prepared and analyzed using SEM, as shown in Figure 4.

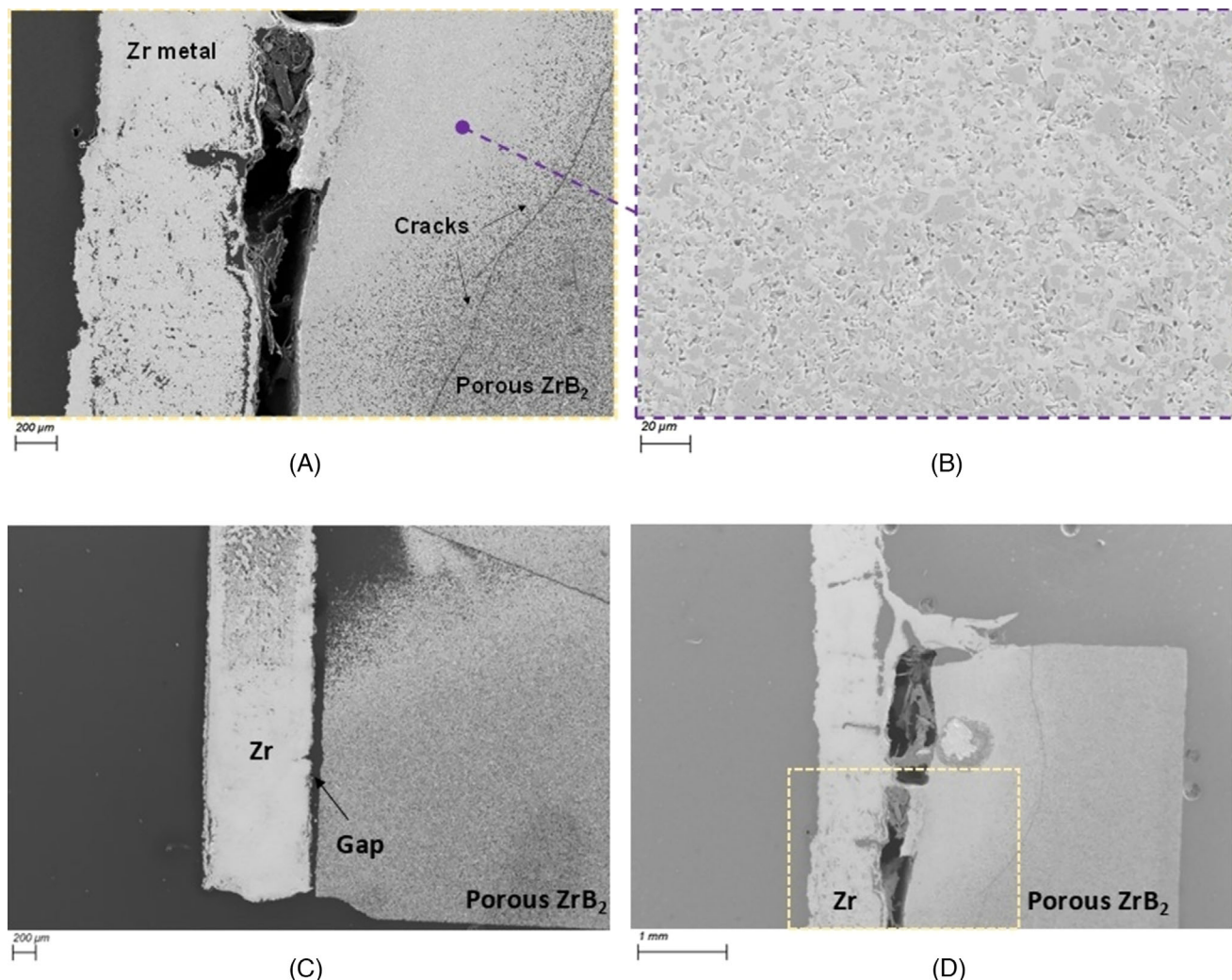


FIGURE 4 SEM analysis of porous  $ZrB_2$  brazed to Zr metal. SEM, scanning electron microscopy.

Figure 4A,C,D shows the macrostructure of the brazed interface. A gap is visible at the interface indicating a failure of the brazed joint. The porous nature of  $ZrB_2$  led to discontinuous adhesion at the interface and the interfacial region shows irregularities.

Figure 4B provides a high-magnification view of the porous  $ZrB_2$  microstructure after brazing. The filler paste infiltrated into the porous structure. The penetrated paste appears light gray in Figure 4B, while  $ZrB_2$  grains are represented in dark gray. This infiltration of the filler paste into the porous  $ZrB_2$  did not improve the mechanical strength of the joint and instead induced localized property modifications. During cooling, the hardening of the infiltrated paste led to the generation of thermal stresses<sup>25</sup> at the interface between the porous zone of  $ZrB_2$  and the infiltrated regions. These stresses induced the formation of cracks around the infiltrated region, as shown in Figure 4A,D. A second porous sample was tested using air compression at 6.5 bar, corresponding to the expected operational

conditions of the final application. After a few minutes of air injection, the Zr tube was detached from the porous  $ZrB_2$  sample, indicating that the brazed joint was not suitable for the intended application. The failure mechanism is attributed to the weak adhesion at the interface due to low wetting of the porous  $ZrB_2$ , paste infiltration altering the local mechanical properties and the thermal expansion mismatch between porous  $ZrB_2$  and Zr metal.

Figure 5 presents the thermal expansion behavior of dense  $ZrB_2$ , porous  $ZrB_2$ , and the Zr metal tube, obtained through dilatometry measurements from room temperature up to 1650°C.

Zr metal has a quite similar nonlinear thermal expansion behavior as dense  $ZrB_2$  and a different behavior from the porous  $ZrB_2$ . To evaluate the thermal compatibility between the materials, the coefficient of thermal expansion (CTE) was extracted from the thermal strain ( $\Delta L/L_0$ ) data over multiple temperature intervals for dense  $ZrB_2$ , porous  $ZrB_2$ , and Zr metal. Table 1 summarizes

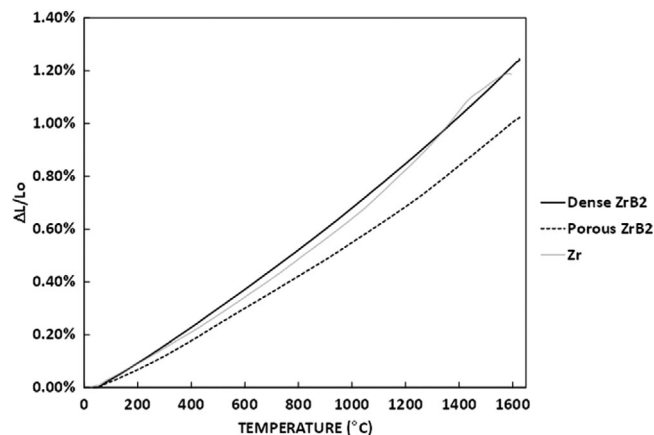


FIGURE 5 Thermal expansion of  $ZrB_2$  materials (porous and dense) and the Zr tube.

TABLE 1 A comparison of CTE values of dense and porous  $ZrB_2$  with that of Zr over multiple temperature ranges.

	Zr	Dense $ZrB_2$	Porous $ZrB_2$
200°C–400°C	5.92E–06	6.74E–06	5.50E–06
600°C–800°C	7.22E–06	7.50E–06	6.07E–06
1000°C–1200°C	9.26E–06	8.40E–06	6.79E–06
1400°C–1600°C	8.98E–06	9.62E–06	8.18E–06

the CTE values across the 200°C–400°C, 600°C–800°C, 1000°C–1200°C, and 1400°C–1600°C ranges.

Zr<sup>26</sup> exhibited a nonlinear increase in CTE with temperature, rising from  $5.92 \times 10^{-6} K^{-1}$  at 200°C–400°C to a peak of  $9.26 \times 10^{-6} K^{-1}$  at 1000°C–1200°C, followed by a slight decrease at higher temperatures. Dense  $ZrB_2$  exhibited a more stable thermal expansion trend, with CTE values ranging from  $6.74 \times 10^{-6}$  to  $9.62 \times 10^{-6} K^{-1}$ , which is consistent with previously reported values in the literature.<sup>27,28</sup> Above 600°C, its CTE closely approaches that of Zr. In contrast, porous  $ZrB_2$  exhibited consistently lower CTEs across all intervals, from  $5.50 \times 10^{-6} K^{-1}$  at 200°C–400°C to  $8.18 \times 10^{-6} K^{-1}$  at 1400°C–1600°C, due to its lower bulk stiffness.

Zr and dense  $ZrB_2$  exhibit a modest CTE mismatch ( $\sim 0.28 \times 10^{-6}$  and  $0.86 \times 10^{-6} K^{-1}$  respectively at 600°C–800°C and 1000°C–1200°C), which minimizes thermal stress and supports interfacial integrity. In contrast, the mismatch with porous  $ZrB_2$  is more pronounced at all temperatures, reaching  $\sim 1.1 \times 10^{-6}$  and  $2.5 \times 10^{-6} K^{-1}$  respectively at 600°C–800°C and 1000°C–1200°C. This confirms the interfacial cracking and discontinuous adhesion observed in the Zr-porous  $ZrB_2$  joints.

This study case demonstrates the feasibility of brazing dense  $ZrB_2$  to Zr metal, achieving a robust and continuous bond with no significant gaps at the interface. The successful joining process can be attributed to the similarity

in thermal expansion coefficients between Zr and dense  $ZrB_2$ , which minimizes stresses during heating and cooling cycles. The continuous interface was observed without measurable discontinuities in the SEM images, along with the absence of delamination or large voids, confirming that the selected brazing parameters were effective in ensuring good wettability and adhesion of the filler material. Additionally, the airtightness test performed under compressed air further validates the mechanical integrity of the joint, highlighting its potential applicability in hypersonic thermal protection systems.<sup>29–34</sup> However, the brazing of porous  $ZrB_2$  presents significant challenges such as thermal expansion mismatch and filler infiltration, which induce a discontinuous bonding of the Zr tube and alter the local material properties, leading to stress accumulation in the ceramic side and generating local cracking while cooling. This issue was exacerbated by the thermal expansion mismatch between Zr and porous  $ZrB_2$ . By optimizing various process parameters such as the paste viscosity, the application of interlayers, and the modification of sintering profile, it is possible to improve bonding performance in this case. These developments will be addressed in future work. For the current application, these findings encourage brazing the Zr to the dense  $ZrB_2$  to transfer the coolant into the porous  $ZrB_2$  via Zr from the supply reservoir to mitigate oxidation effects and reduce the component's temperature. On the other hand, these findings suggest that alternative strategies refine the brazing process in this case, such as optimizing paste viscosity and powder mixing, modifying the sintering profile, incorporating advanced filler materials with improved wetting properties,<sup>24,35–37</sup> lowering thermal expansion differentials and introducing interlayer materials to enhance the adhesion and mechanical performance of brazed porous  $ZrB_2$ –Zr components. From a broader perspective, the insights gained in this study extend beyond hypersonic applications and are relevant to other extreme environments, such as plasma-facing components used in nuclear fusion systems.<sup>38–42</sup> Additionally, further investigation into the long-term performance of the joints under creep-fatigue thermomechanical loading conditions will be crucial in assessing their reliability for real-world applications.

## 4 | CONCLUSION

This paper demonstrated the feasibility of the manufacturing process of a UHTC composite by brazing  $ZrB_2$  with Zr tubes, which serve as channels for coolant delivery in the transpiration cooling technology.

A key objective was to establish a continuous and reliable ceramic-to-metal connection, ensuring structural

integrity and performance stability. To achieve this, brazing conditions—including paste composition and sintering temperature—were carefully optimized to promote effective bonding while minimizing adverse effects on the base materials:

- The joint between dense ZrB<sub>2</sub> and the Zr tube exhibited a continuous bond with no significant gaps, attributed to the similar thermal expansion behavior of both materials at brazing and cooling temperatures.
- In contrast, the joint between porous ZrB<sub>2</sub> and the Zr tube displayed discontinuities due to thermal expansion mismatch.
- The presence of Zr as an active element in the filler paste enhanced wettability but also led to paste infiltration into the porous ZrB<sub>2</sub> microstructure, modifying its local properties and potentially compromising mechanical stability.

Beyond hypersonic applications, the insights gained from this study on ceramic–metal joining are also highly relevant to nuclear fusion technology, where materials must withstand extreme thermal loads, neutron irradiation, and plasma exposure. The development of robust ZrB<sub>2</sub>–metal joints could contribute to advanced cooling systems and thermal protection barriers in plasma-facing components used in fusion reactors, improving the longevity and performance of structural components in harsh operational environments.

## ACKNOWLEDGMENTS

The authors would like to express their sincere gratitude to the reviewers for their valuable feedback and constructive suggestions, which have significantly contributed to improving the quality of the paper.

This research was developed with funding from the Defense Advanced Research Projects Agency. The views, opinions and/or findings expressed are those of the authors and should not be interpreted as representing the official views or policies of the Department of Defense or the U.S. Government.

## ORCID

Younes Belrhiti  <https://orcid.org/0000-0003-4305-1310>

## REFERENCES

1. Irom E, Zakeri M, Razavi M, Farvizi M. ZrB<sub>2</sub>-based ultrahigh-temperature ceramic with various SiC particle size: microstructure, thermodynamical behavior, and mechanical properties. *Int J Appl Ceram Technol.* 2025;22(1):e14855. <https://doi.org/10.1111/ijac.14855>
2. Bai L, Ni S, Jin H, He J, Ouyang Y, Yuan F. ZrB<sub>2</sub> Powders with low oxygen content: synthesis and characterization. *Int J Appl Ceram Technol.* 2018;15(2):508–13. <https://doi.org/10.1111/ijac.12756>
3. Verma V, Cheverikin V, Câmara Cozza R. Review: effect on physical, mechanical, and wear performance of ZrB<sub>2</sub>-based composites processed with or without additives. *Int J Appl Ceram Technol.* 2020;17(6):2509–32. <https://doi.org/10.1111/ijac.13567>
4. Chen Z, Zhao X, Wang H, Shao G, Liu W, Zhang R, et al. Preparation and properties of dense ZrB<sub>2</sub> composite reinforced by elongated SiC and Al<sub>3</sub>BC<sub>3</sub> grains. *Int J Appl Ceram Technol.* 2019;16(6):2190–96. <https://doi.org/10.1111/ijac.13265>
5. Asthana R, Singh M. Evaluation of amorphous Ti brazes to join zirconium diboride-based ultra-high-temperature ceramics to metallic systems. *Int J Appl Ceram Technol.* 2014;11(3):502–12. <https://doi.org/10.1111/ijac.12154>
6. Singh M, Asthana R. Joining of ZrB<sub>2</sub>-based ultra-high-temperature ceramic composites to Cu–Clad–Molybdenum for advanced aerospace applications. *Int J Appl Ceram Technol.* 2009;6(2):113–33. <https://doi.org/10.1111/j.1744-7402.2008.02291.x>
7. McGilvray M, Hermann T, Saad Ifti H, Chakravarthy K, Rocher ME, Williams B, et al. Ultra-high temperature ceramics for transpiration cooling applications in hypersonic vehicles. *Ultra-High Temperature Ceramics: Materials For Extreme Environment Applications V.* ECI Symposium Series. ECI; 2022.
8. Ewenz Rocher M, Hermann T, McGilvray M, Grossman M, Vandeperre L. Measuring the concentration of freestream species on a hypersonic transpiration-cooled stagnation point. *J Spacecr Rockets.* 2022;59(4):1380–87.
9. Ewenz Rocher M, Hermann T, McGilvray M. Oxidation response of transpiration-cooled ZrB<sub>2</sub> on a hypersonic stagnation point. *J Spacecr Rockets.* 2022;59(5):1486–95.
10. Parthasarathy TA, Petry MD, Jefferson G, Cinibulk MK, Mathur T, Gruber MR. Development of a test to evaluate aerothermal response of materials to hypersonic flow using a scramjet wind tunnel. *Int J Appl Ceram Technol.* 2011;8(4):832–47. <https://doi.org/10.1111/j.1744-7402.2010.02515.x>
11. Steyer TE. Shaping the future of ceramics for aerospace applications. *Int J Appl Ceram Technol.* 2013;10(3):389–94. <https://doi.org/10.1111/ijac.12069>
12. Belrhiti Y, Kerth P, McGilvray M, Vandeperre L. Gel-casting for manufacturing porous alumina ceramics with complex shapes for transpiration cooling. *Adv Appl Ceram.* 2023;122(5–8):375–80.
13. Bose S, Akdogan EK, Balla VK, Ciliveri S, Colombo P, Franchin G, et al. 3D Printing of ceramics: advantages, challenges, applications, and perspectives. *J Am Ceram Soc.* 2024;107(12):7879–920. <https://doi.org/10.1111/jace.20043>
14. Afrouzian A, Bandyopadhyay A. Understanding the role of interface in deformation behavior of additively manufactured bimetallic structures of pure metals. *J Mater Res Technol.* 2024;30:70–79. <https://doi.org/10.1016/j.jmrt.2024.03.024>
15. Squires L, Myers MB, Bandyopadhyay A. Radial deposition for mechanical bonding of dissimilar metals in wire arc additive manufacturing. *Adv Eng Mater.* 2025;27(7):2401978. <https://doi.org/10.1002/adem.202401978>
16. Baufeld B, Dutilleul T. Electron beam welding of large components for the nuclear industry. *MATEC Web Conf.* 2019;269:02009.

17. Dawes C. Chapter 5: Laser welding parameters and their effects. In Dawes C, editor. Laser welding. Woodhead Publishing; 1992. p. 78–116. <https://doi.org/10.1533/9781845698843.78>
18. Zhou Z, Chen C. Research advances in the ultrasonic-assisting adhesive bonding. *J Manuf Processes*. 2024;110:134–60. <https://doi.org/10.1016/j.jmapro.2023.12.050>
19. Ravichandran K, Praseetha PK, Arun T, Gobalakrishnan S. Chapter 6: Synthesis of nanocomposites. In: Mohan Bhagyaraj S, Oluwafemi OS, Kalarikkal N, Thomas S, editors Synthesis of inorganic nanomaterials. Micro and nano technologies. Woodhead Publishing; 2018. p. 141–68. <https://doi.org/10.1016/B978-0-08-101975-7.00006-3>
20. Cook GO, Sorensen CD. Overview of transient liquid phase and partial transient liquid phase bonding. *J Mater Sci*. 2011;46(16):5305–23. <https://doi.org/10.1007/s10853-011-5561-1>
21. Hausner S, Wielage B. 12. Brazing of metal and ceramic joints. In: Sekulić DP, editor. Advances in brazing. Woodhead Publishing Series in Welding and Other Joining Technologies. Woodhead Publishing; 2013. p. 361–93. <https://doi.org/10.1533/9780857096500.2.361>
22. Weil KS, Hardy JS, Rice JP, Kim JY. Brazing as a means of sealing ceramic membranes for use in advanced coal gasification processes. *Fuel*. 2006;85(2):156–62. <https://doi.org/10.1016/j.fuel.2005.07.023>
23. Easton D, Zhang Y, Wood J, Galloway A, Robbie MO, Hardie C. Brazing development and interfacial metallurgy study of tungsten and copper joints with eutectic gold copper brazing alloy. *Fusion Eng Des*. 2015;98–99:1956–59. <https://doi.org/10.1016/j.fusengdes.2015.05.033>
24. Guo W, She Z, Xue H, Zhang X. Effect of active Ti element on the bonding characteristic of the Ag(111)/ $\alpha$ -Al<sub>2</sub>O<sub>3</sub>(0001) interface by using first principle calculation. *Ceram Int*. 2020;46(4):5430–35.
25. Goldak J, Lloyd L, Barrett C. Lattice parameters, thermal expansions, and Grüneisen coefficients of zirconium, 4.2 to 1130°K. *Phys Rev X*. 1966;144:478–84. <https://doi.org/10.1103/PhysRev.144.478>
26. Fahrenholtz WG, Hilmas GE, Talmy IG, Zaykoski JA. Refractory diborides of zirconium and Hafnium. *J Am Ceram Soc*. 2007;90(5):1347–64. <https://doi.org/10.1111/j.1551-2916.2007.01583.x>
27. Zimmermann JW, Hilmas GE, Fahrenholtz WG, Dinwiddie RB, Porter WD, Wang H. Thermophysical properties of ZrB<sub>2</sub> and ZrB<sub>2</sub>-SiC ceramics. *J Am Ceram Soc*. 2008;91(5):1405–11. <https://doi.org/10.1111/j.1551-2916.2008.02268.x>
28. Belrhiti Y, Pop O, Germaneau A, Doumalin P, Dupré JC, Harmuth H, et al. Investigation of the impact of micro-cracks on fracture behavior of magnesia products using wedge splitting test and digital image correlation. *J Eur Ceram Soc*. 2015;35:823–29.
29. Hermann T, McGilvray M, Naved I. Performance of transpiration cooled heat shields for re-entry vehicles. *AIAA J*. 2019;58(2):830–41.
30. Ewenz Rocher M, McGilvray M, Hermann TA, Ifti HS, Hufgard F, Eberhart MF, et al. Testing a transpiration cooled zirconium-di-boride sample in the plasma tunnel at IRS. In *AIAA Scitech 2019 forum*. 2019. p. 1552.
31. Ifti HS, Hermann T, Ewenz Rocher M, Doherty L, Hambidge C, McGilvray M, et al. Laminar transpiration cooling experiments in hypersonic flow. *Exp Fluids*. 2022;63(6):102.
32. Naved I, Hermann T, Hambidge C, Ifti HS, McGilvray M, Tirichenko IS, et al. Quantifying the surface heat transfer on transpiration cooled porous materials in laminar and turbulent hypersonic boundary layers; 2022.
33. Hedgecock R, Vandeperre L. Porous UHTCs for transpiration cooling of hypersonic flight. *Ultra-high temperature ceramics: materials for extreme environment applications V*. ECI Symposium Series. 2022.
34. Ifti HS, Hermann T, McGilvray M, Larrimbe L, Hedgecock R, Vandeperre L. Flow characterization of porous ultra-high-temperature ceramics for transpiration cooling. *AIAA J*. 2022;60(5):3286–97.
35. Nogi K. The role of wettability in metal-ceramic joining. *Scr Mater*. 2010;62(12):945–48.
36. Kuhn B, Wessel E, Malzbender J, Steinbrech RW, Singheiser L. Effect of isothermal aging on the mechanical performance of brazed ceramic/metal joints for planar SOFC-stacks. *Int J Hydrogen Energy*. 2010;35(17):9158–65.
37. Xiong H, Chen B, Zhao H, Cheng Y, Ye L. V-containing-active high-temperature brazes for ceramic joining. *Weld World*. 2016;60(1):99–108.
38. Garrison LM, Kulcinski GL, Hilmas G, Fahrenholtz W, Meyer HM. The response of ZrB<sub>2</sub> to simulated plasma-facing material conditions of He irradiation at high temperature. *J Nucl Mater*. 2018;507:112–25. <https://doi.org/10.1016/j.jnucmat.2018.04.016>
39. Bao W, Robertson S, Zhao J-W, Liu J-X, Wu H, Zhang G-J, et al. Structural integrity and damage of ZrB<sub>2</sub> ceramics after 4 MeV Au ions irradiation. *J Mater Sci Technol*. 2021;72:223–30. <https://doi.org/10.1016/j.jmst.2020.09.019>
40. Belrhiti Y, Hamelin C, Knowles D, Mostafavi M. Thermomechanical analysis of tungsten-copper joints for fusion applications using digital image correlation. *Fusion Eng Des*. 2024;206:114608.
41. Galizia P, Uccello A, Ghezzi F, Labate L, Tiribilli B, Hanzel O, et al. Thermal properties of MB<sub>2</sub>-WC (M=Ti, Zr, Hf) and tungsten and their stability after deuterium plasma exposure. *Open Ceram*. 2024;20:100696. <https://doi.org/10.1016/j.oceram.2024.100696>
42. Nuckols L, Parish CM, Baldwin MJ, Meyer HM, Nishijima D, Patino MI, et al. Observation of tantalum deposition and growth on TiB<sub>2</sub> and ZrB<sub>2</sub> from PISCES-RF deuterium and helium plasma exposures. *Nucl Mater Energy*. 2024;39:101641. <https://doi.org/10.1016/j.nme.2024.101641>

**How to cite this article:** Belrhiti Y, Grossman MW, Hedgecock R, McGilvray M, Vandeperre L. Brazing ZrB<sub>2</sub> ultra-high-temperature ceramics to Zr metals for hypersonic thermal protection systems. *Int J Appl Ceram Technol*. 2025;e15161. <https://doi.org/10.1111/ijac.15161>